

See discussions, stats, and author profiles for this publication at: <https://www.researchgate.net/publication/257309115>

The Role of Intact Oleosin for Stabilization and Function of Oleosomes

ARTICLE *in* THE JOURNAL OF PHYSICAL CHEMISTRY B · OCTOBER 2013

Impact Factor: 3.3 · DOI: 10.1021/jp403893n · Source: PubMed

CITATIONS

12

READS

118

8 AUTHORS, INCLUDING:



[Denise Schach](#)

University of Chicago

18 PUBLICATIONS 110 CITATIONS

[SEE PROFILE](#)



[Tobias Weidner](#)

Max Planck Institute for Polymer Research

86 PUBLICATIONS 1,351 CITATIONS

[SEE PROFILE](#)



[Mischa Bonn](#)

Max Planck Institute for Polymer Research

347 PUBLICATIONS 7,587 CITATIONS

[SEE PROFILE](#)



[Thomas Vilgis](#)

Max Planck Institute for Polymer Research

389 PUBLICATIONS 4,261 CITATIONS

[SEE PROFILE](#)

The Role of Intact Oleosin for Stabilization and Function of Oleosomes

Sania Maurer,^{†,‡} Gustav Waschatko,^{||,‡} Denise Schach,^{§,‡} Birgitta I. Zielbauer,[⊥] Jakob Dahl,[⊥] Tobias Weidner,[⊥] Mischa Bonn,[⊥] and Thomas A. Vilgis*,[⊥]

[†]Max Planck Institute for Polymer Research, Ackermannweg 10, 55128 Mainz, Germany

[‡]Department of Food Biotechnology and Food Process Engineering, Technical University of Berlin, Königin-Luise-Str. 22, 14195 Berlin, Germany

^{||}Institute of Pharmacy und Biochemistry, Johannes Gutenberg University Mainz, Johann-Joachim-Becher-Weg 30, 55128 Mainz, Germany

[§]James Franck Institute, 929 East 57th Street, GCIS E139D, Chicago, Illinois 60637, United States

Supporting Information

ABSTRACT: Lipid storage in plants is achieved among all plant species by formation of oleosomes, enclosing oil (triacylglycerides) in small subcellular droplets. Seeds are rich in this pre-emulsified oil to provide a sufficient energy reservoir for growing. The triacylglyceride core of the oleosomes is surrounded by a phospholipid monolayer containing densely packed proteins called oleosins. They are anchored in the triacylglycerides core with a hydrophobic domain, while the hydrophilic termini remain on the surface. These specialized proteins are expressed during seed development and maturation. Particularly, they play a major role in the stabilization and function of oleosomes. To better understand the importance of oleosins for oleosome stabilization, enzymatic digestion of oleosins was performed. This made it possible to compare and correlate changes in the molecular structure of oleosins and changing macroscopic properties of oleosomes. Tryptic digestion cleaves the hydrophilic part of the oleosins, which is accompanied by a loss of secondary structures as evidenced by Fourier-transform infrared and sum frequency generation spectra. After digestion, the ability of oleosins to stabilize oil–water or air–water interfaces was lost. The surface charge and the associated aggregation behavior of oleosomes are governed by interactions typical of proteins before digestion and by interactions typical of phospholipids after digestion.



INTRODUCTION

Oleosomes are subcellular organelles that are expressed during seed development and maturation. These organelles are stabilized by oleosins. Such proteins exhibit a long hydrophobic domain ranging deeply into the lipid core and an umbrella-like hydrophilic region located at the organelle surface. The hydrophilic C- and N-termini provide a pH-dependent net charge. While the hydrophilic region can vary between plants, the long hydrophobic domain, consisting of 70 amino acids (AAs), is strongly conserved across different species.^{1–3} An ensemble of oleosomes forms natural emulsions. These emulsions are stabilized by steric and electrostatic repulsion of oleosins supported by their interactions with different zwitterionic phospholipids (PL).^{4,5}

In the last 2 decades, the cosmetic, pharmaceutical, and food industries discovered that oleosomes can be beneficial as pre-emulsified additives or carriers of valuable (bioactive) ingredients.⁶ However, the current lack of understanding of the link between macro- and microscopic properties of the oleosome emulsions and the respective structure at the molecular level poses a significant barrier to rational, structure-based design of oleosome products. Therefore, the

secondary structure of oleosins has been extensively investigated and controversially debated. The structure of several oleosins was initially predicted by molecular modeling of the amino acid sequences and structural similarities of well-understood animal apolipoproteins.⁷ Murphy et al.⁷ concluded that the central hydrophobic sequence would form a β -strand, even though a hairpin of antiparallel α -helices connected by a proline knot was also proposed for this domain. For the N- and C-terminal regions of the proteins, amphiphilic α -helical structures exposed to the cytosol were suggested. Later predictions found it more probable that no specific structure is preferential, as the terminal regions of the different oleosins are highly variable.³

Circular dichroism (CD) and Fourier-transform infrared (FTIR) spectroscopy have been used to experimentally probe the secondary structure of oleosins from different sources, such as peanut,⁸ rapeseed,^{2,9} sunflower,^{9–11} and safflower.¹⁰ However, only little work has been done to understand how

Received: April 19, 2013

Revised: September 30, 2013

Published: October 2, 2013

the molecular structure of soybean oleosins relates to the oleosome function. Soybeans are the most important protein and oil sources for millions of people, and they are becoming increasingly important for nutritional, health, and care products. Here, we attempt to determine the folding and secondary structures of soybean oleosins, which has not yet been accomplished. We focus on *in situ* studies of oleosins in their native environment, the oleosome. When oleosin-based stabilization of oleosomes is studied, it is often challenging to remove the remaining storage proteins from the sample while keeping the oleosomes intact. Storage proteins in oleosome emulsions can, for example, lead to a wide distribution of droplet sizes,¹² and they generally affect the pH-dependent surface charge and the aggregation behavior of oleosomes. Additional protein content will also interfere with any spectroscopic secondary structure analysis. To solve this problem, we used a modified gentle flotation–centrifugation extraction method at pH 11 developed by Chen and Ono.¹³

To study the structure of the different functional parts of oleosins and their role for oleosome stabilization separately, we enzymatically digested oleosomes. Comparison of samples before and after digestion using spectroscopic and biophysical methods together provides important information about inter- and intramolecular interactions between oleosome components.

For characterizing oleosomes in solution, we have measured their drop size and ζ -potential. Additionally, the rheological properties of o/w-emulsions, prepared by using oleosomes as emulsifier, were analyzed to verify the dramatic stabilizing effect of oleosins. The folding of oleosins within dried oleosomes was characterized by transmission FTIR spectroscopy. For *in situ* spectroscopy under hydrated conditions, we performed sum frequency generation (SFG) experiments of oleosomes at the air–water interface. SFG is a spectroscopy technique used to probe molecular vibrations that are exclusively generated at the interface. Waschatko et al.^{14,15} have shown previously that oleosomes rupture and spread at the air–water interface. They also showed that the resulting layer is a model system to probe interfacial properties of oleosomes. We used SFG to determine the secondary structure of oleosins and to track structural changes upon enzymatic digestion. For comparison, drop-shape analysis was used to show the surface behavior of native and digested oleosomes. This combination of experimental techniques provided information about oleosin function at different length scales, ranging from the mesoscopic down to the molecular level.

MATERIAL AND METHODS

For all preparation steps, ultrapure water, filtered with a Millipore device (Billerica, MA/USA), was used. For oleosome digestion, trypsin NB from porcine pancreas (Cat. No. 37294, tryptic activity $\geq 50 \mu\text{kat/g}$ (Ph.Eur.), Serva, Germany) was used, which contains mainly trypsin but also minor contents of chymotrypsin, elastase, and nonproteolytic activity, which is usually lipolytic. Proteolytic activity and oleosome protein composition were confirmed by SDS-PAGE; lipolytic activity was confirmed by thin layer chromatography (TLC) with soybean oil emulsions. Solvents were purchased from Sigma-Aldrich (Steinheim, Germany). The buffers and salts used are described in previous publications.^{14,15} The control emulsion for FTIR spectroscopy contained 0.75% lecithin (Serva, Heidelberg, Germany) and 15% soybean oil (Sojola, Hamburg,

Germany) emulsified in ultrapure water with an IKA T18 basic Ultra Turrax (15 600 rpm, 1 min).

Oleosome Isolation and Purification. Isolation of soybean oleosomes was performed by a modified aqueous flotation–centrifugation method proposed by Chen and Ono.¹³ Dried soybeans (Davert) bought from a local supermarket were soaked in deionized water at 4 °C for at least 20 h. After this, soaked beans were separated from the excessive water, and fresh water was added to obtain a 10% soybean-to-water ratio. The mixture was ground in a Vorwerk Thermomix TM31 at a speed of 10 200 rpm for 90 s. Raw soy milk was obtained by filtering the resulting slurry through two layers of Kimtech science precision wipes (21 × 11 cm², Kimberly Clark). To remove residual storage proteins, 25% sucrose (w/w) was added to the soy milk and the pH was adjusted to 11.0 with 1 mol L⁻¹ NaOH solution. The solution was divided into portions of 50 mL and centrifuged (15 000g, 4 °C) for at least 5 h. The resulting cream layer was taken off with a spoon, resuspended in a 20% sucrose solution of pH 11.0 and centrifuged anew. This washing step was performed twice. The purified oleosome cream layers were collected and dispersed in 50 mL of deionized water. Subsequently, the oleosome solution was dialyzed in a cellulose tube (MWCO 12 000–14 000, *b* = 45 mm, wall thickness = 20 μm) from ZelluTrans (Roth, Karlsruhe, Germany) to remove the sucrose used for the extraction of the oleosomes.

Trypsin Digestion. One milligram of trypsin from porcine pancreas was added to 1 mL of dialyzed, isolated, intact oleosomes (85% water content). The digestion was performed at 25 °C for 1 h at 500 rpm in a HLC ThermoMixer MKR 13.

FTIR Spectroscopy. The FTIR spectra were recorded on a Bruker Vertex 70 equipped with a DLaTGS detector in transmission mode. All spectra were recorded at room temperature. A transmission cell with a CaF₂ window was used. Each spectrum was averaged for 40 scans at a resolution of 2 cm⁻¹. As a background reference, the bare CaF₂ window was used, and the sample chamber was purged with dry air for 10 min. After purification, the soy oleosome emulsions of either native or trypsin-digested oleosomes were centrifuged for 30 min to again separate the aqueous phase from the oleosome cream layer. Twenty milligrams of the oleosome cream layer was spread on a CaF₂ window and dried overnight under a stream of dry air to remove excess water. D₂O instead of H₂O was used as a solvent to compare the respective spectra with each other. Here, the cream layer after the first centrifugation step was redissolved, centrifuged anew, and dissolved again two times in D₂O to provoke the H/D exchange.

Before measurements, the chamber was purged with dry air for 10 min. The spectra of aqueous emulsions consisting of water, soybean oil, and soybean lecithin (emulsions with and without trypsin) were compared with the native and digested oleosome spectra. These control samples were prepared and dried on the transmission windows in the same way as the native oleosomes. The exact peak positions were identified by the minimum positions in the second derivatives. The derivative spectra were obtained using the Savitzky–Golay algorithm with a degree of 2 and a width of 9 points using the software package OPUS. A linear baseline correction was applied to the spectra. The amide I region was fitted with a sum of profiles consisting of 50% Lorentzian shape and 50% Gaussian shape¹⁶ using the Levenberg–Marquardt algorithm.¹⁷ The resonance positions inferred from the second derivative spectra were fixed, and the full width at half-maximum (fwhm)

and the band area were determined. For better comparison, the spectrum of the trypsin-digested oleosomes was multiplied by a factor of 4.5 in the figures. Bands were assigned to secondary structure according to refs 10, 18, and 19, which allowed quantification of the relative contributions of different structural components to the overall structure. The resonance positions are reported with an error margin of $\pm 2 \text{ cm}^{-1}$.

SFG Spectroscopy. For the sum frequency generation (SFG) experiments, broadband infrared pulses (fwhm of $\sim 200 \text{ cm}^{-1}$) generated by an OPG/OPA (TOPAS, Light Conversion), which was pumped by $\sim 2 \text{ W}$ average power of 800 nm pulses from a Spitfire Ace (Spectra Physics) amplified laser system (1 kHz, $\sim 40 \text{ fs}$ fwhm), were used. In addition, approximately 0.5 W of the laser output passed through an etalon that generated a narrow band visible pulse (fwhm bandwidth of $\sim 15 \text{ cm}^{-1}$) to provide the spectral resolution of the experiment. The broadband infrared pulse ($\sim 3.5 \mu\text{J}$) provided a spectral window of 200 cm^{-1} , centered around 1700 cm^{-1} in the amide I region. A trough ($3 \times 80 \times 40 \text{ mm}$) was filled with 6 mL of 5 mM PBS buffer (pH 7). $26.7 \mu\text{L}$ of native or digested aqueous oleosome solution (1440 mg/L) was injected into the subphase to yield a total concentration of about 6.4 mg/L (surface pressure measurements at different oleosome concentrations, including this one, are described in a previous work¹⁵). The samples were allowed to equilibrate for 20 min before the SFG measurements. The visible and infrared beams overlapped spatially and temporally at the solution surface. The incident angles of the visible (VIS) and infrared (IR) beam were $\sim 35^\circ$ and $\sim 40^\circ$ with respect to the surface normal. The VIS beam was focused down to a diameter of approximate $400 \mu\text{m}$. The SFG light was spectrally dispersed by a monochromator and detected by an electron-multiplied charge coupled device (EMCCD, Andor Technologies). Spectra were recorded using p-polarized SFG, VIS, and IR beams with 600 s of acquisition time. The spectra were then corrected for the background and normalized with a reference spectrum generated by the nonresonant SFG signal of a silver surface. The background signal was also recorded with 600 s of acquisition time while blocking the IR pulse. Lorentzian band shapes were fitted to the spectra according to the relation

$$I \propto |\chi^{(2)}|^2 \propto \left| A_{\text{NR}} e^{-i\phi_{\text{NR}}} + \sum_n \frac{A_n}{\omega_n - \omega_{\text{IR}} - i\Gamma_n} \right|^2$$

in a manner that was consistent with the imaginary part of the susceptibility, $|\chi^{(2)}|$, obtained using the maximum entropy method (MEM), which is a numerical method to retrieve the phase information in spectra.²⁰ Here, A_{NR} is the amplitude and ϕ_{NR} the phase of nonresonant signal, A_n is the amplitude of resonant signal, ω_n is the resonant frequency, ω_{IR} is the infrared frequency, and Γ_n is the width of transition.

Droplet Size Distribution. The cumulative volume distribution ($Q_3 (\%)$) is defined as the average volume of droplets that are equal to or smaller than a specific droplet size x . By using a laser diffraction analyzer (Horiba LA-950, Retsch Technology, Germany), we measured Q_3 of native and trypsin-digested oleosomes dispersed in buffer solutions of varying pH value. To avoid multiple scattering effects, the oleosomes were diluted as appropriate with buffer solutions. The Sauter mean diameter $d_{32} = 6V_d/A_d$, where V_d is the volume of the droplet and A_d is the droplet area, was determined as the characteristic average droplet size. The diffractive data was calculated using a predefined optical model for liquid disperse formulations of

small droplets ($\leq 10 \mu\text{m}$) according to Mie theory. However, the refractive index of oleosomes is not yet known and could not be readily determined due to the constituents' inhomogeneity. Therefore, the real parts of the refractive indices (n) were estimated according to literature values. These are 1.47 for soybean oil²¹ and range from 1.594 to 1.630 for common proteins (e.g., casein, lactoglobulin, lysozyme).²² Test trials, where the measured scattering intensities were compared with the calculated ones (variance $\chi^2 = 0.45$), verified appropriate indices of 1.6 (real part) and 0 (imaginary part). The ionic strength of the oleosome–buffer solution was kept constant at 10 mM, and measurements were conducted at room temperature. Droplet size distributions were measured in triplicate using three different samples.

The droplet size distribution of emulsions prepared from native and digested oleosomes was also examined by laser diffraction. Here, the same procedure as described above was performed. The measurements were conducted in duplicate using two different samples.

ζ -Potential. Dispersions of native and trypsin-digested oleosomes were diluted using buffer solutions (10 mM sodium chloride, varying pH) to avoid multiple scattering effects. Diluted oleosome dispersions were filled into a cuvette, which was then placed into the chamber of a Zetasizer Nano ZS (Malvern, Germany). The ζ -potential was measured on the basis of laser Doppler anemometry (LDA) and deduced from the electrophoretic mobility of the droplets according to the Helmholtz–Smoluchowski equation, eq 1. By application of an external electric field, the charged disperse droplets move with different velocity detected by laser light scattering. Based on this approximation and the assumption that oleosomes are spherical with a smooth surface, the ζ -potential, ζ , is derived from the shear viscosity, η , the velocity, v , the external electrical field, E , and the dielectric constant, ϵ .²³

$$\zeta = \frac{4\pi\eta v}{E\epsilon} \quad (1)$$

Measurements were conducted in duplicate from two freshly prepared samples at 25°C .

Interfacial Activity. The dynamic properties of native and digested oleosome layers at the air–water interface were investigated by applying axisymmetric drop shape analysis (ADSA). An automated drop tensiometer OCA20 (Dataphysics GmbH, Germany) was used to determine the interfacial surface pressure of native and trypsin-digested oleosomes dispersed in different solutions of varying pH values (2, 5.3, and 8) and at constant ionic strength (10 mM, NaCl). A high speed frame grabber (200 frames/s) recorded the shape changes of the pendant drop. Static measurements were conducted in a temperature-controlled chamber ($T = 22.8 \pm 0.2^\circ\text{C}$). To prevent evaporation and changes in the drop volume due to air current, the syringe placed in the automated dosing system was enclosed with a cuvette, which was filled with a few drops of water and tightly sealed with Parafilm. The drop was formed with a dosage rate of $5 \mu\text{L}/\text{s}$ at the tip of a stainless steel hydrophobized capillary. The injected drop volume of varying concentrations (15.6–1560 mg/L) of native and trypsin-digested oleosome dispersions was $15 \pm 0.3 \mu\text{L}$. To ensure that the drop volume could equilibrate for each measurement equally, a waiting time of 30 s after the drop formation was taken before the measurements. Changes in drop shape were monitored for 600 s. A software belonging to the drop tensiometer OCA20 was used to fit the Gaussian–Laplace

equation of capillary to the experimental drop shape coordinates and thus to be able to determine the interfacial tension.²⁴ By subtraction of the obtained surface tension of the pendant drop from the surface tension of pure water ($\sigma_0 = 72.65 \text{ mN/m}$ at 22.8°C), the surface pressure (in mN/m) was calculated according to $\pi = \sigma_0 - \sigma$ and plotted against the time. Measurements were conducted at least in duplicate.

Rheology of Emulsions. Fifty grams of soybean oil was slowly added to 25 mL of a 23.3% soybean oleosome dispersion (native and digested) in 5 mM Tris/NaCl ($I = 5 \text{ mM}$), pH 8, buffer and homogenized with an IKA T18 basic Ultra Turrax (15 600 rpm, 4 min). Rheological measurements of the emulsions were performed directly after preparation.

A Bohlin Gemini 200 with a coaxial cylinder measuring system (inner diameter 25 mm, outer diameter 27.5 mm) was used to determine the viscosity of a 12 g emulsion depending on shear rate employing the Searle method. The shear rate $\dot{\gamma}$ was varied from 0.0002 to 400 s^{-1} . The measurement time for each point was 5 s. A shear rate dependent delay time, t_d (equilibration time between measurement points), was used, with $t_d = 120 \text{ s}$ for the lowest shear rate; $t_d(\dot{\gamma})$ was calculated in the following way:

$$t_d(\dot{\gamma}) = 120 \text{ s} \frac{0.0002 \text{ s}^{-1}}{\dot{\gamma}}$$

An upward shear rate ramp was followed by a downward one to check for hysteresis effects. All measurements were performed at 25°C .

RESULTS AND DISCUSSION

Oleosome Purification, Digestion, and Characterization. The efficiency of the purification with regard to the removal of the storage proteins has been verified by SDS-PAGE (Figure 1). Thereby, three bands corresponding to the size of four soybean oleosins known in the protein database UniProtKB²⁵ (isoforms P29530 and P29531, 23–24 kDa; C3VHQ8, 17–18 kDa, C6SZ13, 15–16 kDa) and evident in transcription could be confirmed. Oleosins of plant oleosomes were first described in the 1970s and are extensively reviewed by Huang et al.¹ Additionally, the total nitrogen content of isolated soybean oleosomes was determined by the Dumas method, revealing a protein content of 4.4–5.8% (calculated factor for the conversion of total nitrogen content to protein content for soybean oleosins was 5.9).

Trypsin from porcine pancreas, which exhibits proteolytic and lipolytic activity, both also relevant in plants during seed germination, as well as in the human gastrointestinal tract, was used. Lipolysis and proteolysis of oleosomes^{26,27} may interfere with each other in physiological processes. On the one hand, proteolysis cleaves the outer domains of the oleosins, which are the barrier preventing coalescence and a potential anchor for lipases.²⁶ On the other hand, lipases hydrolyze triacylglycerides (TAG) into fatty acids (FFA), as well as mono- and diglycerides (MG and DG), which can stabilize a lipid droplet interface.²⁸ After digestion with commercial trypsin only protein fragments smaller than 6 kDa were visible in the SDS-PAGE (Figure 1), due to the proteolytic activity of trypsin, chymotrypsin, and elastases. Furthermore, the electrophoretic separation of the commercial trypsin (lane 1) displayed proteins with molecular weights between 38 and 62 kDa, which is in accordance with the size of pancreatic lipases, for

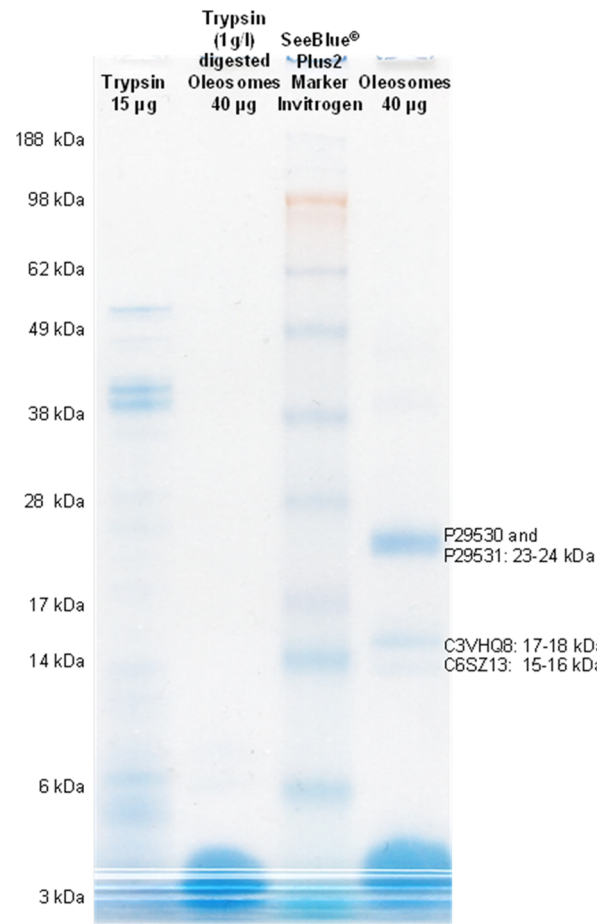


Figure 1. Commassie stained SDS-PAGE gel of purified soybean oleosomes before and after digestion with trypsin. Oleosomes were digested with 1 mg/mL of commercial trypsin at 25°C for 1 h in a ThermoMixer. The trypsin lane (15 μg) shows high molecular weight proteins between 38 and 62 kDa, like pancreatic lipase.

example, P00591 (porcine pancreatic triacylglycerol lipase, 50 kDa).

TLC, with mobile phase A of Soxhlet extraction residues of native oleosomes, showed phospholipids ($R_f = 0.2\text{--}0.5$),²⁹ which are not extractable with pentane. This confirmed that the PL had been bound to the intact oleosin proteins.⁵ Hydrolysis products of TAG were detected at $R_f = 0$ for MG, $R_f = 0.3$ for DG, and $R_f = 0.5$ for FFA (mobile phase B).³⁰

FTIR Spectroscopy. FTIR spectroscopy was applied to estimate the secondary structure contents of native and trypsin-digested oleosomes. Since trypsin was shown to cleave the hydrophilic from the hydrophobic part at lysine and arginine, a comparison of spectra from native and protease treated oleosomes can yield information about the secondary structures of the two protein regions. The native samples contain secondary structure elements of all protein parts, whereas the spectra of trypsin-digested oleosomes are expected to contain only structural elements of the remaining central hydrophobic part. To exclude water bands, all samples were dried on CaF_2 windows before the measurements. The spectra of native and digested oleosomes as well as dried aqueous soybean oil/lecithin emulsions have common bands around $2800\text{--}3050$, 1456 , and $1200\text{--}1100 \text{ cm}^{-1}$ (data not shown), which have been attributed to C–H stretch, C–H deformation, and C–O bonding vibrational modes of the TAGs, respectively.¹⁰

Moreover, all spectra show a prominent band near 1745 cm^{-1} , which was assigned to the carbonyl stretch vibration of TAG esters¹⁰ (see Figure 2).

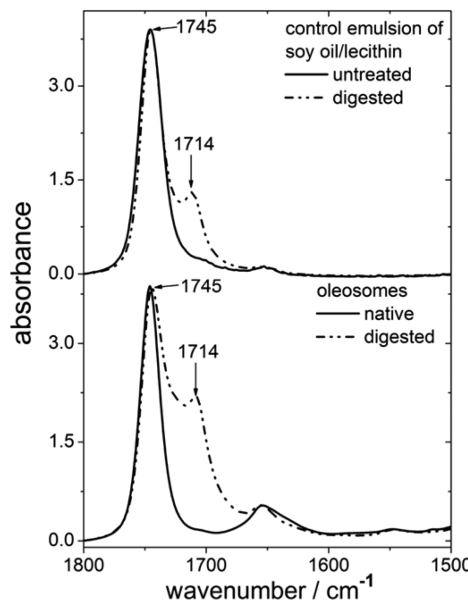


Figure 2. Absorbance spectra of native (lower solid trace) and trypsin-digested (containing lipases) soybean oleosomes (lower dashed trace) compared with absorbance spectra of untreated (upper solid trace) and trypsin treated soybean oil lecithin emulsions (upper dashed trace).

A comparison of spectra of native oleosomes with spectra of soybean oil/lecithin control samples showed a number of bands related to lipid molecules such as TAG. The oil/lecithin control samples were also treated with commercial trypsin to check

whether the enzymes or lipid digestion products generate additional bands (see Figure 2, upper dashed trace). A strong additional band around 1714 cm^{-1} was detected, which also appeared in the spectra of digested oleosomes (see Figure 2, lower dashed trace). The band did not appear in samples treated with trypsin (Cat. No. 37291, Serva, Heidelberg, Germany) of higher purity without lipolytic activity. Hence this band was assigned to the carboxylic acid group (fatty acids) carbonyl stretching (see Table 1). This is an indication that the commercial trypsin contained not only pancreatic proteases but also lipases.

The spectra of the control samples exhibit a very weak band around 1650 cm^{-1} , which could be attributed to amide I vibrational modes of residual proteins in the control emulsion. However, this weak band does not seem to increase after digestion, indicating that enzymes did not significantly add to the protein content.

The spectra of all oleosome samples showed broad protein related absorption bands in the amide I region centered around 1656 cm^{-1} (Figure 3, solid trace) and in the amide II region around 1550 cm^{-1} . Second derivative analysis (data not shown) was employed to determine the exact band positions for the secondary structure analysis. The spectrum of native oleosomes exhibits a strong signal around 1656 cm^{-1} . The second derivative indicates that this signal might consist of two contributions, one at 1657 cm^{-1} and one at 1653 cm^{-1} . In D_2O (data not shown), the band at 1657 cm^{-1} is unaltered whereas the band at 1653 cm^{-1} shifts to 1645 cm^{-1} as expected for unordered structures.³¹ Thus, the band at 1657 cm^{-1} was assigned to α -helical structures, accounting for 47% of the total amide intensity, and the band at 1653 cm^{-1} was assigned to unordered structures (see Table 1). Shoulders on both sides of the main absorbance were found at 1624 , 1634 , and 1682 cm^{-1} , which can be attributed to β -sheet structures. These modes represent 31% of the amide content, which is in line with

Table 1. Parameters Resulting from Band Fit of FTIR Spectra in the Amide I Region for Native and Digested Soybean Oleosomes

soybean ^a				safflower ^b		sunflower ^c	
band (cm^{-1})	fhwm (cm^{-1})	area (%)	assignment	band (cm^{-1})	area (%)	band (cm^{-1})	area (%)
Native							
624	18	6	intermolecular β -sheet	1618	9	1621	6
1634	24	13	antip. β -sheet/ β -sheet	1628/1641	5/26	1628/1639	4/22
1653	30	17	random coil				
1657	34	47	α -helix	1657	50	1654	33
1673	31	5	β -turns	1671	6	1668	23
1682	26	12	β -sheet	1682	3	1678	2
			β -sheet/ β -turns	1690	1	1687	10
1746 ^d			carbonyl stretch of ester				
Digested							
				1618	6	1617	7
1633	25	21	antip. β -sheet/ β -sheet	1629/1641	5/20	1632/1640	13/8
1656	22	73	α -helix	1656	60	1655	59
			β -turns	1670	5	1667	11
1680	14	6	β -sheet	1680	4	1681	2
1714 ^d			carbonyl stretch of carboxyl group				
1746 ^d			carbonyl stretch of ester				

^aParameters resulting from FTIR spectra shown in Figures 2 and 3 and tentative assignment of fitted bands to secondary structures according to literature.^{10,18,19} ^bFor comparison, parameters reported in Lacey et al.¹⁰ obtained from FTIR spectra of native and protease digested safflower oleosins. ^cFor comparison, parameters reported in Lacey et al.¹⁰ obtained from FTIR spectra of native and protease digested sunflower oleosins.

^dAssignment of bands to carbonyl stretching modes of lipid content are reported.

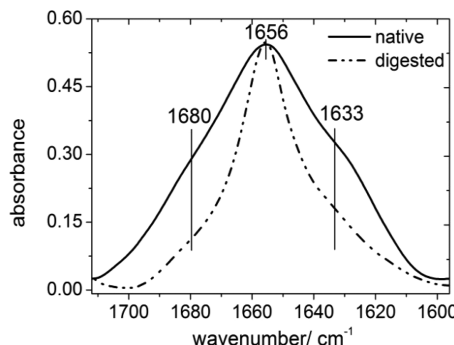


Figure 3. Absorbance spectra in the amide I region of native (solid trace) and trypsin-digested (low lipase activity) soybean oleosomes (dashed trace).

findings of Lacey et al.¹⁰ A further band that arises at 1673 cm^{-1} , accounting for 5% of the amide signal, most likely originates from β -turns.

To determine the secondary structure of only the hydrophobic protein domain after digestion, the emulsion was centrifuged to remove the cleaved, hydrophilic protein fragments. Afterward, the aqueous phase was discarded, and the FTIR-spectra of the remaining cream layer containing the trypsin-digested oleosomes were recorded (Figure 3, dashed trace). In these experiments, trypsin without lipolytic activity was used to avoid spectral confusion with lipid-based digestion products. When the spectrum of the native oleosomes is compared with that of digested oleosomes, it becomes apparent that the overall band shapes strongly differ, in agreement with previous observations by Lacey et al.¹⁰ In the second derivative spectrum of digested oleosomes, the central absorbance around 1656 cm^{-1} no longer consists of two bands, and it is significantly narrower, although weak shoulders on both sides of the central band remain visible. The hydrophobic oil environment of the remaining hydrophobic protein part prevents a verification of the band assignments by D_2O exposure. However, based on the narrow peak and the above assignments for the native sample, the 1656 cm^{-1} band can most likely be assigned to α -helical structures. The α -helical signal accounts for $\sim 73\%$ of the total amide intensity. There is no significant amount of random structures present in these samples. Contributions attributed to β -sheet structures are also less pronounced (27% of the total amide intensity). The predominance of α -helical structures after protease treatment has been observed before,¹⁰ showing that the hydrophobic oleosin domains are most likely dominated by α -helix. The cleaved hydrophilic protein fraction consequently seems to be dominated by random coils and β -sheets.

Droplet Size Analysis and ζ -Potential. The stability of colloidal droplets against aggregation can be determined via droplet size (Sauter mean diameter, d_{32} (μm)), cumulative volume distribution, Q_3 (vol (%)), and the ζ -potential, ζ (mV), measurements. Oleosomes are micellar spherical droplets with a lipid core that is surrounded by a monolayer of PL and completely covered by the umbrella-like oleosins. Moreover, soybean oleosomes are known to be the smallest oil bodies compared with oleosomes of other seeds. Because of the different amino acid sequence of the oleosin hydrophilic parts exposed at the oleosome surface, the net surface charge distribution of an oleosome depends on the pH value and ionic strength of the solution.³² Therefore, droplet size measurements have been performed at different pH values. To highlight

the effect of pH values close to the isoelectric point of native oleosins on the droplet size distribution of the oleosomes, measurements at intermediate pH values between 4 and 6 were performed. This additional data is presented in the Supporting Information (Figure S.1). However, the following discussion includes all measured pH values.

Droplet size measurements in the pH range of 2–4.2 and 5.7–8 revealed that soybean oleosomes are relatively small (60 vol % of droplets with $d < 0.2\text{ }\mu\text{m}$; Figure 4A,B (pH 2–8),

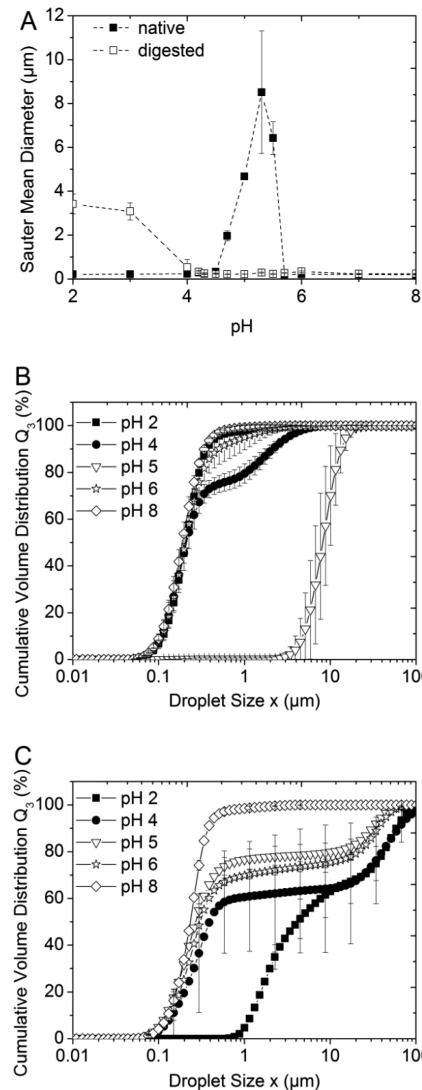


Figure 4. Sauter mean diameter (μm) of native and trypsin-digested oleosomes in terms of pH (A) and cumulative volume distribution, Q_3 (%), plotted against the droplet size (μm) of native (B) and digested oleosomes (C) (with representative error bars).

Figure S.1 (pH 4.2–5.7), Supporting Information). However, at their isoelectric point ($\text{pI} \approx 5.3$), 90 vol % of oleosomes form aggregates larger than $5\text{ }\mu\text{m}$. At pH values close to the pI (pH 4.3 and 5.7), the mean droplet size of $0.2\text{ }\mu\text{m}$ is only slightly higher ($d_{32} = 0.2 \pm 0.2\text{ }\mu\text{m}$) than that at low (2–4) or high (6–8) pH values (Figure 4A). However, the cumulative volume distribution reveals an increasing volume of oleosomes larger than $0.2\text{ }\mu\text{m}$ (Figure 4B (pH 4–5); Figure S.1 (pH 4.2–5.5), Supporting Information) and therefore a higher tendency to aggregate for pH values close to the pI . In general, the further

apart the pH is from the pI the more the oleosomes repel each other. Close to the pI , the remaining Coulombic (electrostatic) repulsion is not sufficiently strong to overcome attraction (e.g., hydrophobic and van der Waals interactions) and aggregation occurs.

In contrast to similar studies,¹² showing the formation of larger aggregates in a broad pH range from 3 to 6, the pH range in which the oleosomes are unstable is relatively narrow (pH 4.7 ($d_{32} = 2.0 \mu\text{m}$) to pH 5.5 ($d_{32} = 6.5 \mu\text{m}$); Figure 4A). This discrepancy might result from different purification procedures during the aqueous extraction process. The centrifugation of oleosomes at pH = 11 used here provided a better separation from residual storage proteins. Creaming stability tests of oleosomes containing some remaining residues of storage proteins showed a pronounced shift of the pI to around pH = 4 and a significantly broader pH range of oleosome aggregation.^{12,13}

The digestion of oleosomes causes a loss of structural integrity resulting in a different droplet size distribution that is affected by pH differently than that for intact oleosomes. In the pH range of 4.2–8, the average mean droplet size of $<0.3 \mu\text{m}$ is comparable to the average droplet size of native oleosomes in the high acidic (pH 2–4) and weak acidic to alkaline (pH 5.7–8) region. However, the volume distribution is, in contrast to intact oleosomes, relatively inhomogeneous, as 20 (pH 5.3) to 40 vol % (pH 4) of the droplets are significantly larger than 5 μm (Figure 4C). In the very acidic region (pH 2 and 3), droplets of digested oleosomes form aggregates or coalesce into droplets of an average size of 3.0 μm (Figure 4A). Almost 50% of those are larger than 5.0 μm (Figure 4C).

With regard to the multicomponent mixture of protein fragments and lipids (TAG, PL, FFA, MG, and DG) in the dispersion after digestion, it is difficult to evaluate the effects that might have contributed to the increase in droplet size in the acidic region and the broadening of the droplet size distribution. The different pH values at which the largest droplets occur (Figure 4A) are most probably caused by the cleavage of the hydrophilic and charged protein part from the oleosome surface. This alters the electrical charge distribution of the oleosome surfaces, which is then predominately based on the different zwitterionic properties of the polar head groups of the PL and FFA and no longer on the charge of the oleosin. ζ -Potential measurements and creaming stability tests indicate that oleosomes with PL monolayers coalesce while protein-covered oleosomes form flocculates at critical pH values. It is therefore concluded that the removal of the hydrophilic protein termini not only changes the surface charge but also removes a steric barrier against coalescence.

To better understand the destabilization phenomenon, the ζ -potential was analyzed to quantify the electric double layer of intact and digested oleosomes relevant for evaluation of colloidal interaction and colloidal stabilization. The ζ -potential for native oleosomes changes from $+32 \pm 1.2 \text{ mV}$ at pH 2 to $-24 \pm 1.6 \text{ mV}$ at pH 8 reaching zero at pH 5, which is consistent with the pI of the oleosin (Figure 5). This behavior, which is typical for proteins adsorbed at oil droplets,³³ indicates that oleosins remain at the oleosome surface despite the relatively harsh conditions during the extraction and purification procedure.

A different behavior is observed for digested oleosomes. The ζ -potential in the acidic region is almost the same as that for intact oleosomes (+30 mV) but becomes 0 mV at pH 3.2 and shifts to more negative values ($-75 \pm 3.3 \text{ mV}$ at pH 8) in the

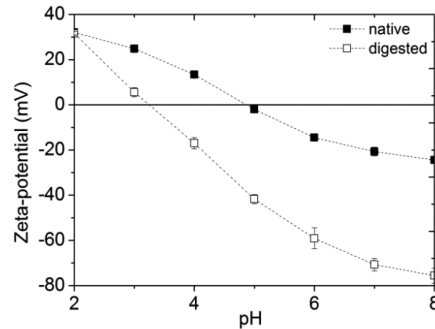


Figure 5. ζ -Potential (mV) of native and digested oleosomes measured in terms of pH.

alkaline region. This pH dependency of the ζ -potential is consistent with that of the so-called parental emulsions stabilized with PL and FFA,³⁴ here particularly driven by phosphatidylcholine, the major phospholipid in oleosomes.³⁵ The higher number of negatively charged phosphate head groups of PL, that is, phosphatidylethanolamine³⁶ and phosphatidylserine in the alkaline region, might contribute to more negative values. However, as shown in the droplet size distribution (Figure 4C), the higher negative charges do not seem to be sufficient to overcome attractive forces, and coalescence might have occurred. Although native oleosomes are stable from a ζ -potential of approximately 15 mV on, one has to take into account that they are additionally sterically stabilized by native oleosins on their interface. On the other hand, for digested oleosomes, even a low probability to approach each other, as expected for intermediate ζ -potentials, might lead to coalescence due to the lower stability of their interface. Only at high ζ -potentials (-75 mV at pH 8), the probability for collisions is sufficiently reduced to stabilize the droplets. In order to further investigate the relation between ζ -potential and coalescence in the digested oleosome system, comparative measurements with PL stabilized emulsions exhibiting similar sizes and droplet volume fractions are planned.

SFG Spectroscopy. Sum frequency generation spectroscopy was employed to probe the structure and composition of the surface active layer forming at an air–water interface after oleosomes have ruptured upon reaching the interface. Figure 6 shows spectra of the amide I region. The spectrum of native oleosomes after rupture exhibits a distinct strong band at 1747 cm^{-1} and a weaker band at 1664 cm^{-1} (Figure 6, upper trace). The strong 1747 cm^{-1} band is also present in the FTIR spectra and was therefore assigned to the carbonyl stretch mode of TAG (Table 2). The band at 1664 cm^{-1} can be attributed to amide I protein modes. In reference to previous reports of amide I band assignments, this signal was tentatively assigned to β -turns or symmetric stretch of parallel β -sheet structures.^{37–39} The α -helical oleosin segments are not visible in the spectra. The absence of helical structure in the spectra can be explained by two scenarios: (i) the α -helical structures are not present at the interface or (ii) the net SFG signal is canceled out because of antiparallel α -helical orientations. Antiparallel orientations of helix motives are common in extended helical coils. SFG is a coherent technique, and signals from groups having opposite orientations (i.e., opposite phase) are not detected in the far field. Ward et al.⁴⁰ have shown this effect for methyl groups. SFG signal cancellation has been observed for β -strands on surfaces⁴¹ and a theoretical analysis of the SFG

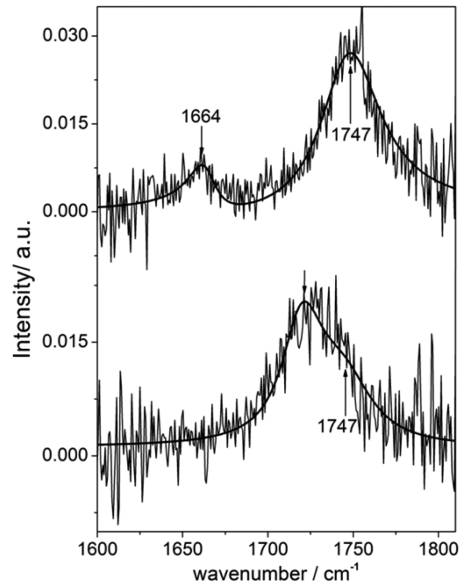


Figure 6. SFG spectra measured under ppp polarization conditions and band fit of native (upper trace) and digested soybean oleosomes (lower trace) 1200 s after injection of oleosomes. Conditions: 6.4 mg/L oleosomes in 5 mM phosphate buffer, pH 7.

Table 2. Parameters Resulting from Band Fit of SFG Spectra for Native and Digested Soy Oleosomes (Figure 6) under ppp Polarization Conditions

	A_{NR}	Φ_{NR}	ω_n^{-1} (cm ⁻¹)	Γ_n^{-1} (cm ⁻¹)	A_n (au)	tentative assignment
native	−0.01	2.80	1663.8	26.7	0.84	β -sheet structures
			1746.7	42.9	3.44	carbonyl stretch of ester
digested	0.03	2.80 ^a	1719.2	34.7	3.44	carbonyl stretch of carboxyl group
			1746.7 ^a	42.9 ^a	−3.08	carbonyl stretch of ester

^aparameters which were fixed during the fitting procedure.

response of helix structure shows that a very similar effect is expected for helices with opposite orientations.⁴² Since the presence of both α -helices and β -sheets is evident from the FTIR analysis and because of the consistent interpretation of the hydrophobic part as an antiparallel α -helix structure in the literature,¹⁰ the latter possibility is likely here.

For digested oleosomes, the amide I band is completely absent (Figure 6, lower trace). This observation is in line with the results from FTIR spectroscopy. The protein fractions exposed to the water have been cleaved by proteases. A statement about whether the hydrophobic antiparallel domains (antiparallel α -helices) aggregate (scenario 2 in Figure 10) or dissolve in lipid domains at the air–water interface (scenario 1 in Figure 10) cannot be made here.¹⁵

It should be noted that, in this picture, we assume that the hydrophobic domain within the oleosome is protected from trypsin cleavage for two reasons: (i) there are no trypsin cleavage sites in the hydrophobic domain (amino acids 77–130),²⁸ and (ii) trypsin is unable to penetrate into the oil phase and, thus, cannot cleave the hydrophobic domain. Our

interpretation of the SFG data as antiparallel helices is at this point, rather speculative. However, the low accessibility and susceptibility of the hydrophobic domain to trypsin cleavage makes it a likely scenario here.

Furthermore, a small but distinct shift of the carbonyl stretching mode related to the TAG esters is observed. Analysis of this signal by means of the maximum entropy method (MEM) exhibited two signals with opposite phases (i.e., opposite orientations). Therefore, two bands can be identified, the remaining band at 1747 and an additional one at 1719 cm^{−1}. The additional signal is tentatively assigned to the carbonyl stretching mode of FFA obtained after cleavage of the TAG by lipase. This result is again in agreement with the observation made using FTIR spectroscopy. In contrast to the results obtained from FTIR spectroscopy, the signal of this band in the SFG spectra seems to be much stronger than the signal from residual intact TAG, which decreases significantly, whereas this band in FTIR spectra remains strong. There seems to be a difference in composition after spreading of oleosome constituents after their rupture at the air–water interface compared with the bulk emulsion. This can be explained by the higher surface concentration of FFA (due to TAG hydrolysis) and PL (due to digestion of binding sites to oleosins), which are both forming monolayers and domains at the air–water interface, visible with Brewster angle microscopy.¹⁴

Interfacial Behavior. The interfacial behavior of intact and digested oleosomes was investigated by axisymmetric drop shape analysis (ADSA). In previous studies,^{14,15} the adsorption mechanisms and behavior of oleosomes at the interface were investigated by using a film balance, but the analysis by ADSA additionally allows for the detection of very fast diffusion processes at the beginning of the kinetics under relatively stable measurement conditions. Here, diffusion of oleosomes to the air–water interface is driven by Brownian motion while buoyancy forces are the driving forces for film balance measurements. Together with information from molecular spectroscopy at the air–water interface (SFG), representative kinetics of intact and digested oleosomes (78 mg/L, pH 2) recorded with ADSA (Figure 7) are discussed.

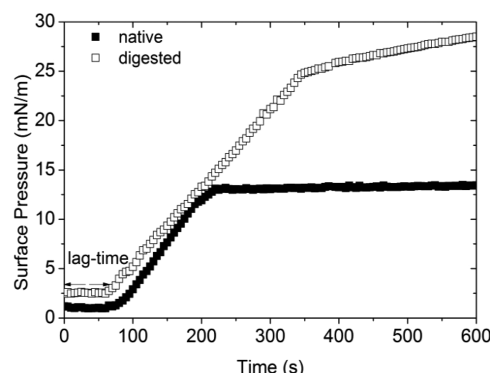


Figure 7. Surface pressure (mN/m) of 78 mg/L of intact and digested oleosomes diluted in a buffer solution of pH 2.

As soon as a sufficient amount of oleosomes has diffused from the bulk phase to the lower interphase, rupture of oleosomes and release of their components occur, and the surface pressure steeply increases. The lag time, the sharp increase, and then the kink in the surface pressure development can be explained by typical PL monolayer behavior,⁴³

comparable to a Langmuir (trough) isotherm. During the lag time, oleosomes burst at the air–water interface and release parts of their PL (native oleosomes) or PL and FFA (digested oleosomes). The oleosome components spread on the surface of the droplet. Initially, the distribution of oleosome components at the air–water interface is comparable with a gaseous phase, which is then going step by step in a coexistence with the liquid expanded phase. When more oleosomes diffuse to the surface and/or are disrupted, the initial free surface is diminished (decreasing the area per molecule) and the monolayer of PL and FFA reaches the liquid expanded phase (sharp increase). The leveling-off of the surface pressure after the kink indicates a depletion of oleosomes in the bulk phase as all oleosomes have diffused to the interface. For intact oleosomes, where a large amount of oleosin–lipid conjugates¹⁵ fill the surface, the free PL can be considered to be in the condensed + liquid expanded coexistence phase.⁴³ For digested oleosomes, the final surface pressure (28.5 mN/m) is considerably higher than that for native ones (13.3 mN/m). This is induced by the enzymatic cleavage of oleosin–PL binding sites leading to the release of more free PL and FFA after rupture but with a dominating influence of the PL on the surface pressure.⁴⁴ However, FFA are detected in SFG spectra (Figure 6), which were recorded 20 min after the injection of oleosomes. Additionally, some authors indicate⁴⁵ that adsorption of special proteins (with an affinity for PL monolayers) can change PL head and tail interactions, leading to less tilted aliphatic chains in the condensed phase and increasing the lipid packing efficiency.

Rheology of Emulsions. The macroscopic emulsifying properties and their molecular origin were probed by preparing emulsions from native (emulsion N) and digested oleosomes (emulsion D) and measuring their shear rate dependent viscosities. The molecular changes of enzymatic digestion on the surface of oleosomes determine interactions between the emulsion droplets and are apparent in macroscopic properties, such as rheological behavior. Emulsions N and D show a shear thinning behavior (Figure 8A). However, the viscosity of emulsion N is about 3 orders of magnitude higher than that of emulsion D. A plot of shear stress versus shear rate for increasing and decreasing shear rates shows almost no hysteresis (Figure 8B), meaning that no substantial irreversible structural breakdown occurred for higher shear rates.⁴⁶ On the other hand, emulsion N has a yield stress of about 10 Pa, whereas emulsion D does not exhibit any yield stress.

The viscosity of an emulsion strongly depends on the volume fraction of the dispersed phase and for concentrated emulsions ($\phi > 0.6$) on the droplet size,⁴⁷ with larger droplets leading to lower viscosities, and their size distribution.⁴⁸ Here, the oil volume fraction is 0.75 in both cases (estimated using a density of 0.93 kg/L for soybean oil and assuming the volume of the oleosomes to be made up almost exclusively of oil). Therefore, a difference in droplet sizes would be expected to have an influence on the viscosity. Laser diffraction measurements (Figure 9) indeed show a different droplet size distribution of emulsions N and D. In general, droplets of emulsion D are larger than those of emulsion N, with Sauter mean diameters of $35.9 \pm 0.1 \mu\text{m}$ and 14.0 ± 0.1 , respectively. Additionally, the cumulative volume distribution of emulsion D is bimodal, because a volume fraction of approximately 2% of the droplets is smaller than $2.5 \mu\text{m}$, while all droplets of emulsion N are larger than $3 \mu\text{m}$.

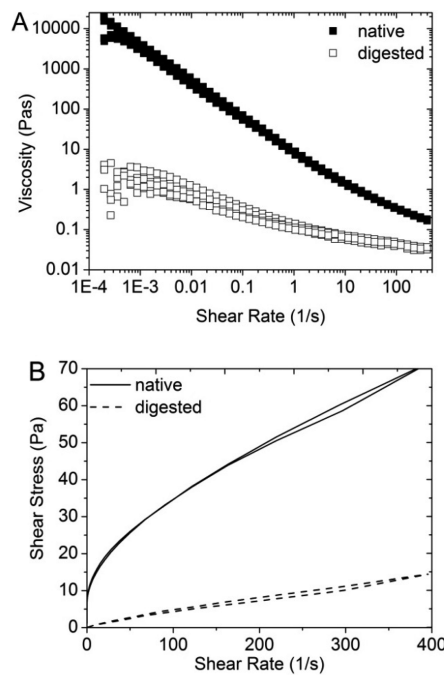


Figure 8. Viscosity (A) and shear stress (B) versus shear rate for emulsions prepared from native and digested oleosomes.

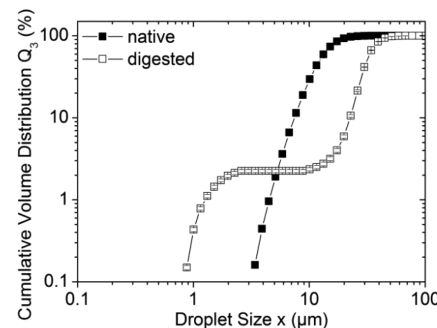


Figure 9. Cumulative volume distribution of emulsions prepared from native and digested oleosomes.

The resulting drop size of an emulsion is determined by the equilibrium between drop breakage and drop–drop coalescence.⁴⁹ Roughly speaking, drop breakage is determined by the ratio of shear forces occurring during emulsification to the Laplace pressure ($2\sigma/R$) of the droplets. The shear forces important for the droplet breakup are equal in the two emulsions compared here due to the identical emulsification process. However, the surface tension can be lowered more by the components present in digested oleosomes (Figure 7) leading to a lower Laplace pressure. Thus, a smaller droplet size could be expected for emulsions from digested oleosomes. On the other hand, the stability against coalescence is expected to be lower for emulsion D, due to the more fluid interfacial layer and missing steric stabilizing effects from native oleosins, thus leading to larger droplets. The droplet size distribution suggests a lower stability against coalescence for droplets between 2 and $10 \mu\text{m}$ for emulsion D.

At high volume fractions of the dispersed phase, droplets get deformed by contact with neighbors,⁴⁶ leading to a strong increase in the elastic modulus of the emulsion.⁵⁰ This deformation occurs above a critical volume fraction, which is larger for droplets with a uniform size distribution than for

those with a broader one, because for the latter the smallest droplets can fit in between the larger ones.⁴⁸ This leads to a reduction in viscosity for more polydisperse emulsions⁵¹ having the same volume fraction of material.

Yield stress occurs if the droplets are so densely packed that they have to deform first before they can move past each other. The force needed for deforming the droplets therefore depends on the volume fraction and size distribution of the droplets (how much they are deformed by their neighbors) as well as on the deformability of the droplet itself. The different droplet size distributions of the two different emulsions could already explain a higher yield stress for emulsion N. However, for the latter also a stronger elastic layer at the interface is expected due to the presence of proteins, which can interact with each other. On the other hand, the FFA and PL present in emulsions from digested oleosomes are not able to interact and lead to easily deformable droplets.

Further investigations of droplet size distribution as well as stress and strain dependent rheological investigations of emulsions at different pH and emulsifier concentration are planned to further elucidate the underlying mechanisms of oleosome emulsifying capacities.

CONCLUSIONS

A comparison of the molecular composition, the surface structure, the colloidal stability, and the interfacial activity of native and enzymatically digested soybean oleosomes was performed for the first time. It has been shown that the stability of oleosomes, as well as their ability to stabilize oil–water emulsions, crucially depends on the unique structure of native oleosins. Figure 10 summarizes the role oleosins play in determining the physicochemical properties and stability of soybean oleosomes, which is consistent with the presented data.

SFG spectra of native oleosomes spread on the water surface revealed the presence of ordered oleosins, phospholipids, and TAG molecules. SFG spectra of the interfacial layer derived from digested oleosomes do not contain any amide I bands, which is probably a result of the loss of hydrophilic oleosin regions. The hydrophobic domain within the oil layer remains invisible in the spectra, most likely due to an antiparallel α -helical configuration. These results are corroborated by FTIR data.

Time-dependent surface pressure measurements show a lag time with constant surface pressure, then exhibit a strong increase, and finally reach a constant level. This process is most likely determined by the kinetics of oleosomes rupturing at the interface, as well as phase transitions occurring in the interfacial layer of the droplet. PL phase transitions leading to regions with different rates of increase in surface pressure are likely to occur if more and more oleosomes release their surface active components, which spread out on the interface. The plateau of the surface tension curve may also be related to the depletion of oleosomes in the bulk phase. The behavior of whole oleosomes at the air–water interface should be compared with studies performed with purified oleosins,^{52,53} which, however, have to face the problem of insolubility and aggregation of the oleosins in water.

Oleosin degradation decreases the stabilization of oleosome emulsions, which is reflected by the increasing polydispersity of the oleosome size, decreasing elasticity of the droplet interfacial layer, and changing interaction between droplets. As a consequence of digestion, which is obviously accompanied by

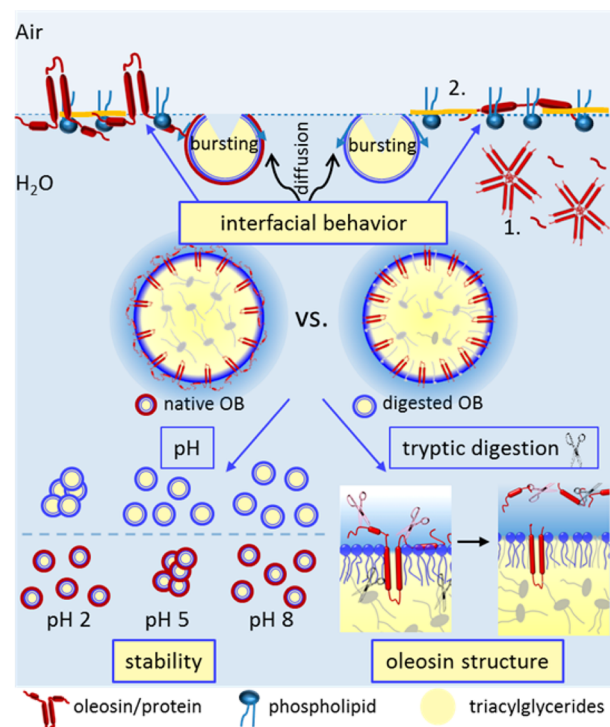


Figure 10. Schematic overview of the effects of oleosin digestion on structure and function of oleosomes. Bursting and the subsequent spreading of the components of digested oleosomes might result in two different scenarios.⁸

changes in molecular composition and structure of the oleosome surface, the ζ -potential and the aggregation behavior of oleosomes change. Thereby, the steric stabilization through the oleosin termini disappears and coalescence of the oil droplet is likely to occur.

This study could further reinforce the expected role of intact oleosins on the stabilization and function of oleosomes. Moreover, it points out the drastic changes in the physical character of oleosomes when the hydrophilic termini are cleaved by tryptic digestion. This correlation is essential when lipids need to be accessed and consumed in plants during seed germination or in mammalian gastrointestinal digestion. With regard to food oil refinery, enzyme-assisted aqueous extraction, which is ecologically and environmentally friendly and healthier than common solvent extraction methods, can achieve higher oil yields when oil is extracted from isolated oleosomes.⁵⁴

The aim to better understand the nature of these proteins is even more relevant with particular respect to biodegradability, which is a general issue when dealing with emulsions used for biomedical, biotechnological, and food applications. As formerly in the case of membrane proteins, a suitable solubilization and reconstitution method remains to be developed. We hope the present study inspires and provides useful information toward this possible development.

ASSOCIATED CONTENT

Supporting Information

Detailed presentation of the cumulative droplet volume distribution of oleosomes at intermediate pH values close to the oleosin isoelectric point. This material is available free of charge via the Internet at <http://pubs.acs.org>.

AUTHOR INFORMATION

Corresponding Author

*Phone: +49 6131 379143. Fax: +49 6131 379340. E-mail: vilgis@mpip-mainz.mpg.de.

Author Contributions

[‡]S.M., G.W. and D.S. contributed equally to this work.

Notes

The authors declare no competing financial interest.

ACKNOWLEDGMENTS

We thank Dr. Michael Schleeger and Dr. Ellen Backus for fruitful discussions regarding IR and SFG spectra interpretation. We are also grateful to Dr. Ann Junghans for her comments and advice during the preparation of this manuscript. Additionally, many thanks are given to Prof. Dr. Ing. Heike Schuchmann and Philipp Stähle from the Karlsruher Institute for Technology (KIT, Germany) where we used the Horiba LA-950 for the droplet size measurements. Further, we thank Prof. Dr. Stephan Drusch and Frederic Tamm from the Technical University of Berlin for providing the pendant drop tensiometer.

REFERENCES

- (1) Huang, A. H. C. Oil Bodies and Oleosins in Seeds. *Annu. Rev. Plant Physiol. Biol.* **1992**, *43*, 177–200.
- (2) Li, M.; Smith, L. J.; Clark, D. C.; Wilson, R.; Murphy, D. J. Secondary Structures of a New Class of Lipid Body Proteins from Oilseeds. *J. Biol. Chem.* **1992**, *267*, 8245–8253.
- (3) Tzen, J. T. C.; Huang, A. H. C. Surface-Structure and Properties of Plant Seed Oil Bodies. *J. Cell Biol.* **1992**, *117*, 327–335.
- (4) Alexander, L. G.; Sessions, R. B.; Clarke, A. R.; Tatham, A. S.; Shewry, P. R.; Napier, J. A. Characterization and Modelling of the Hydrophobic Domain of a Sunflower Oleosin. *Planta* **2002**, *214*, 546–551.
- (5) Purkrbova, Z.; Jolivet, P.; Miquel, M.; Chardot, T. Structure and Function of Seed Lipid Body-Associated Proteins. *C. R. Biol.* **2008**, *331*, 746–754.
- (6) Bhatla, S. C.; Kaushik, C.; Yadav, M. K. Use of Oil Bodies and Oleosins in Recombination Protein Production and Other Biotechnological Applications. *Biotechnol. Adv.* **2010**, *29*, 293–300.
- (7) Murphy, D. J.; Keen, J. N.; Osullivan, J. N.; Au, D. M. Y.; Edwards, E. W.; Jackson, P. J.; Cummins, I.; Gibbons, T.; Shaw, C. H.; Ryan, A. J. A Class of Amphipathic Proteins Associated with Lipid Storage Bodies in Plants - Possible Similarities with Animal Serum Apolipoproteins. *Biochim. Biophys. Acta* **1991**, *1088*, 86–94.
- (8) Jacks, T.; Hensarling, T.; Neucere, J.; Yatsu, L.; Barker, R. Isolation and Physicochemical Characterization of the Half-Unit Membranes of Oilseed Lipid Bodies. *J. Am. Oil Chem. Soc.* **1990**, *67*, 353–361.
- (9) Li, M.; Keddie, J. S.; Smith, L. J.; Clark, D. C.; Murphy, D. J. Expression and Characterization of the N-terminal Domain of an Oleosin Protein from Sunflower. *J. Biol. Chem.* **1993**, *268*, 17504–17512.
- (10) Lacey, D. J.; Wellner, N.; Beaudoin, F.; Napier, J. A.; Shewry, P. R. Secondary Structure of Oleosins in Oil Bodies Isolated from Seeds of Safflower (*Carthamus Tinctorius* L.) and Sunflower (*Helianthus Annuus* L.). *Biochem. J.* **1998**, *334*, 469–477.
- (11) Millchip, M.; Tatham, A. S.; Jackson, F.; Griffiths, G.; Shewry, P. R.; Stobart, A. K. Purification and Characterization of Oil Bodies (Oleosomes) and Oil-Body Boundary Proteins (oleosins) from the Developing Cotyledons of Sunflower (*Helianthus annus* L.). *Biochem. J.* **1996**, *314*, 333–337.
- (12) Iwanaga, D.; Gray, D. A.; Fisk, I. D.; Decker, E. A.; Weiss, J.; McClements, D. J. Extraction and Characterization of Oil Bodies from Soy Beans: A Natural Source of Pre-Emulsified Soybean Oil. *J. Agric. Food Chem.* **2007**, *55*, 8711–8716.
- (13) Chen, Y.; Ono, T. Simple Extraction Method of Non-Allergenic Intact Soybean Oil Bodies that Thermally Stable in an Aqueous Medium. *J. Agric. Food Chem.* **2010**, *58*, 7402–7407.
- (14) Waschatko, G.; Junghans, A.; Vilgis, T. A. Soy Milk Oleosome Behaviour at the Air-Water Interface. *Faraday Discuss.* **2012**, *158*, 157–169.
- (15) Waschatko, G.; Schiedt, B.; Vilgis, T. A.; Junghans, A. Soybean Oleosomes Behavior at the Air–Water Interface. *J. Phys. Chem. B* **2012**, *116*, 10832–10841.
- (16) Arrondo, J. L. R.; Goñi, F. M. Structure and Dynamics of Membrane Proteins as Studied by Infrared Spectroscopy. *Prog. Biophys. Mol. Biol.* **1999**, *72*, 367–405.
- (17) Marquardt, D. W. An Algorithm for Least-Squares Estimation of Nonlinear Parameters. *J. Soc. Ind. Appl. Math.* **1963**, *11*, 431–441.
- (18) Byler, D. M.; Susi, H. Examination of the Secondary Structure of Proteins by Deconvolved FTIR Spectra. *Biopolymers* **1986**, *25*, 469–487.
- (19) Susi, H.; Byler, D. M. Resolution-Enhanced Fourier Transform Infrared Spectroscopy of Enzymes. *Methods Enzymol.* **1986**, *130*, 290–311.
- (20) Sovago, M.; Vartiainen, E.; Bonn, M. Determining Absolute Molecular Orientation at Interfaces: A Phase Retrieval Approach for Sum Frequency Generation Spectroscopy. *J. Phys. Chem. C* **2009**, *113*, 6100–6106.
- (21) Zeleny, L.; Neustadt, M. H.: Rapid Determination of Soybean-Oil Content and of Iodine Number of Soybean Oil, U. S. Department of Agriculture Technical Bulletin, Washington, DC, 1940; Vol. 748, pp 1–23.
- (22) McMeekin, T. L.; Groves, M. L.; Hipp, N. J. Refractive Indices of Amino Acids, Proteins, and Related Substances. In *Amino Acids and Serum Proteins*; Stekol, J. A., Ed.; Advances in Chemistry Series; American Chemical Society: Washington, DC, 1964; Vol. 44, pp 54–66.
- (23) Attard, P.; Antelmi, D.; Larson, I. Comparison of the Zeta Potential with the Diffuse Layer Potential from Charge Titration. *Langmuir* **2000**, *16*, 1542–1552.
- (24) Cheng, P.; Li, D.; Boruvka, L.; Rotenberg, Y.; Neumann, A. W. Automation of Axisymmetric Drop Shape Analysis for Measurements of Interfacial Tensions and Contact Angles. *Colloids Surf. A* **1990**, *43*, 151–167.
- (25) UniProt Consortium. Reorganizing the protein space at the Universal Protein Resource (UniProt). *Nucleic Acids Res.* **2012**, *40*, D71–D75.
- (26) Beisson, F.; Ferté, N.; Bruley, S.; Voultaury, R.; Verger, R.; Arondel, V. Oil-Bodies as Substrates for Lipolytic Enzymes. *Biochim. Biophys. Acta, Mol. Cell Biol. Lipids* **2001**, *1531*, 47–58.
- (27) Allen, D. K.; Tao, B. Y. Kinetic Characterization of Enhanced Lipase Activity on Oil Bodies. *Bioprocess Biosyst. Eng.* **2007**, *30*, 271–279.
- (28) Day, J. P. R.; Rago, G.; Domke, K. F.; Velikov, K. P.; Bonn, M. Label-Free Imaging of Lipophilic Bioactive Molecules during Lipid Digestion by Multiplex Coherent Anti-Stokes Raman Scattering Microspectroscopy. *J. Am. Chem. Soc.* **2010**, *132*, 8433–8439.
- (29) Samoto, M.; Maebuchi, M.; Miyazaki, C.; Kugitani, H.; Kohno, M.; Hirosuka, M.; Kito, M. Abundant Proteins Associated with Lecithin in Soy Protein Isolate. *Food Chem.* **2007**, *102*, 317–322.
- (30) Vinarov, Z.; Petkova, Y.; Tcholakova, S.; Denkov, N.; Stoyanov, S.; Pelan, E.; Lips, A. Effects of Emulsifier Charge and Concentration on Pancreatic Lipolysis. 1. In the Absence of Bile Salts. *Langmuir* **2012**, *28*, 8127–8139.
- (31) Haris, P. I.; Severcan, F. FTIR Spectroscopic Characterization of Protein Structure in Aqueous and Non-aqueous Media. *J. Mol. Catal. B: Enzym.* **1999**, *7*, 207–221.
- (32) Nylander, T.; Arnebrant, T.; Bos, M.; Wilde, P. Protein/Emulsifier Interactions. In *Food Emulsifiers and Their Applications*; Hasenhuettl, G. L., Hartel, R. W., Eds.; Springer: New York: 2008; pp 89–171.
- (33) Guzey, D.; Kim, H. J.; McClements, D. J. Factors Influencing the Production of O/W Emulsions Stabilized by β -Lactoglobulin–Pectin Membranes. *Food Hydrocolloids* **2004**, *18*, 967–975.

- (34) Wabel, C. Influence of lecithin on structure and stability of parenteral fat emulsions. Ph.D. Thesis, Friedrich-Alexander-University, July 1998.
- (35) Garcia, J. M.; Quintero, L. C.; Mancha, M. Oil Bodies and Lipid Synthesis in Developing Soybean Seeds. *Phytochemistry* **1988**, *27*, 3083–3087.
- (36) Petelska, A. D.; Figaszewski, Z. A. Interfacial Tension of Bilayer Lipid Membrane Formed from Phosphatidylethanolamine. *Biochim. Biophys. Acta, Biomembr.* **2002**, *1567*, 79–86.
- (37) Fu, L.; Ma, G.; Yan, E. C. Y. In Situ Misfolding of Human Islet Amyloid Polypeptide at Interfaces Probed by Vibrational Sum Frequency Generation. *J. Am. Chem. Soc.* **2010**, *132*, 5405–5412.
- (38) Nguyen, K. T.; King, J. T.; Chen, Z. Orientation Determination of Interfacial β -Sheet Structures in Situ. *J. Phys. Chem. B* **2010**, *114*, 8291–8300.
- (39) Baugh, L.; Weidner, T.; Baio, J. E.; Nguyen, P. C. T.; Gamble, L. J.; Slayton, P. S.; Castner, D. G. Probing the Orientation of Surface-Immobilized Protein G B1 Using ToF-SIMS, Sum Frequency Generation, and NEXAFS Spectroscopy. *Langmuir* **2010**, *26*, 16434–16441.
- (40) Ward, R. N.; Davies, P. B.; Bain, C. D. Orientation of Surfactants Adsorbed on a Hydrophobic Surface. *J. Phys. Chem.* **1993**, *97*, 7141–7143.
- (41) Weidner, T.; Apte, J. S.; Gamble, L. J.; Castner, D. G. Probing the Orientation and Conformation of alpha-Helix and beta-Strand Model Peptides on Self-Assembled Monolayers Using Sum Frequency Generation and NEXAFS Spectroscopy. *Langmuir* **2010**, *26*, 3433–3440.
- (42) Nguyen, K. T.; Le Clair, S. V.; Ye, S. J.; Chen, Z. Orientation Determination of Protein Helical Secondary Structures Using Linear and Nonlinear Vibrational Spectroscopy. *J. Phys. Chem. B* **2009**, *113*, 12169–12180.
- (43) Kaganer, V. M.; Möhwald, H.; Dutta, P. Structure and Phase Transitions in Langmuir Monolayers. *Rev. Mod. Phys.* **1999**, *71*, 779–819.
- (44) Levy, M. Y.; Benita, S.; Baszkin, A. Interactions of a Non-ionic Surfactant with Mixed Phospholipid-Oleic Acid Monolayers. Studies under Dynamic Conditions. *Colloids Surf.* **1991**, *59*, 225–241.
- (45) Dahmen-Levison, U.; Brezesinski, G.; Möhwald, H. Specific Adsorption of PLA2 at Monolayers. *Thin Solid Films* **1998**, *327*–329, 616–620.
- (46) Bruijne de, D. W.; Bot, A. Fabricated Fat-Based Foods. In *Food Texture Measurement and Perception*; Rosenthal, A. J., Ed.; Aspen Publishers: Gaithersburg, MD; 1999; pp 185–227.
- (47) Pal, R. Shear Viscosity Behavior of Emulsions of Two Immiscible Liquids. *J. Colloid Interface Sci.* **2000**, *225*, 359–366.
- (48) Lacasse, M.-D.; Grest, G. S.; Levine, D.; Mason, T. G.; Weitz, D. A. Model for the Elasticity of Compressed Emulsions. *Phys. Rev. Lett.* **1996**, *76*, 3448–3451.
- (49) Tcholakova, S.; Denkov, N. D.; Danner, T. Role of Surfactant Type and Concentration for the Mean Drop Size during Emulsification in Turbulent Flow. *Langmuir* **2004**, *20*, 7444–7458.
- (50) Mason, T. G.; Bibette, J.; Weitz, D. A. Elasticity of Compressed Emulsions. *Phys. Rev. Lett.* **1995**, *75*, 2051–2054.
- (51) Mason, T. G.; Rai, P. K. Shear-Induced Elastification of Concentrated Emulsions Probed by Sinusoidal Amplitude Variation Rheometry. *J. Rheol.* **2003**, *47*, 513–533.
- (52) Roux, É.; Baumberger, S.; Axelos, M. A. V.; Chardot, T. Oleosins of *Arabidopsis thaliana*: Expression in *Escherichia coli*, Purification, and Functional Properties. *J. Agric. Food Chem.* **2004**, *52*, 5245–5249.
- (53) Nikiforidis, C. V.; Ampatzidis, C.; Lalou, S.; Scholten, E.; Karapantsios, T. D.; Kiosseoglou, V. Purified Oleosins at Air-Water Interfaces. *Soft Matter* **2013**, *9*, 1354–1363.
- (54) Towa, L. T.; Kapchie, V. N.; Wang, G.; Hauck, C.; Wang, T.; Murphy, P. A. Pilot Plant Recovery of Soybean Oleosome Fractions by an Enzyme-Assisted Aqueous Process. *J. Am. Oil Chem. Soc.* **2011**, *88*, 733–741.